



ELSEVIER

Microelectronics Journal 33 (2002) 1043–1051

Microelectronics
Journal

www.elsevier.com/locate/mejo

Identification of biological tissue using chirped probe THz imaging

B. Ferguson^{a,b,c,*}, S. Wang^a, D. Gray^{b,c}, D. Abbott^b, X.-C. Zhang^a

^aDepartment of Physics, Applied Physics and Astronomy, Rensselaer Polytechnic Institute, Troy, NY 12180, USA

^bDepartment of Electrical and Electronic Engineering, Centre for Biomedical Engineering, The University of Adelaide, Adelaide, SA 5005, Australia

^cCRC for Sensor, Signal and Information Processing, Technology Park, Mawson Lakes Boulevard, Mawson Lakes, SA 5095, Australia

Received 1 February 2002; revised 4 July 2002; accepted 1 August 2002

Abstract

We consider the application of pulsed THz imaging systems in biomedical diagnostics and mail/package inspection. The sub-millimetre spectroscopic measurements obtained from T-ray systems contain a wealth of information about the sample under test. We demonstrate that different types of tissue can be classified based on their terahertz response measured with the chirped probe pulse technique. We demonstrate the performance of a quadratic classifier using linear filter models for feature extraction in the discrimination between different tissues.

Modern THz systems are hindered by the slow acquisition speed. The chirped probe pulse technique offers a significant improvement in this context. We present the terahertz responses of biological samples measured using a chirped probe pulse, and discuss the problem of data processing and extracting sample characteristics.

© 2002 Elsevier Science Ltd. All rights reserved.

Keywords: Terahertz; T-ray imaging; Chirped pulse; Linear-filter modelling; Classification

1. Introduction

Terahertz imaging is a relatively new addition to the wide array of available imaging modalities. It utilises the terahertz, or far-infrared, region of the electromagnetic spectrum and is based upon the increasingly popular technique of terahertz time-domain spectroscopy (THz-TDS). The unique properties of THz radiation allow terahertz imaging to fill niches that are unreachable using other techniques. THz spectroscopy systems are seeing application in semi-conductor characterisation [1], gas sensing [2] and molecular probing [3]. Terahertz imaging has been demonstrated for imaging flames [4], leaf moisture content [5], skin burn severity [4], tooth cavities [6] and skin cancer [7]. Several excellent reviews of THz-TDS [8] and T-ray imaging [9,10] are available.

Electro-optic (EO) detection of a terahertz pulse using a chirped probe pulse was first demonstrated by Jiang and Zhang [11]. This novel technique allows the full terahertz waveform to be measured simultaneously rather than

requiring a stepped motion stage to scan the temporal profile. This provides a significant reduction in the acquisition time and greatly extends the applicability of terahertz systems in situations where the sample is dynamic or moving. Indeed, single shot measurements have been demonstrated for measuring the transmitted terahertz response using a single femtosecond light pulse [12].

We have utilised the chirped probe pulse technique to acquire images of *in vitro* tissue samples and this paper presents classification results based on the spectroscopic information obtained from these measurements. The chirped pulse technique is not without its drawbacks, and the reduction in temporal resolution has been noted by other authors [13,14]. We present spectra obtained using the chirped pulse method and discuss the limitations imposed in the frequency domain.

Signal processing techniques for terahertz systems is a relatively unexplored area, however, work has been reported in determining optimal techniques for de-noising [15,16], extracting material constants [17,18] and gas mixture analysis [19]. This paper adds to this important field by considering linear modelling as a means of feature extraction with a goal of classifying samples based on their terahertz responses. This has particular application in a medical imaging setting where extracted diagnostic

* Corresponding author. Address: Department of Electrical and Electronic Engineering, Centre for Biomedical Engineering, The University of Adelaide, Adelaide, SA 5005, Australia. Tel.: +61-8-8303-6296; fax: +61-8-8303-4360.

E-mail address: bradleyf@eleceng.adelaide.edu.au (B. Ferguson).

information is required to aid the medical practitioner in assessing the patient.

This paper begins by summarising the field of T-ray imaging. Section 2 reviews the available technologies for performing T-ray imaging and Section 2.1 describes the principles of THz imaging with a chirped probe beam and details our experimental setup. We then introduce the signal processing algorithms employed to process the data from the chirped imaging system. Section 3 provides details on the linear filter models and the classification scheme which was developed. The results of this analysis are given in Section 4. Finally Section 5 summarises the results and suggests directions for future research.

2. THz imaging

Terahertz imaging was first proposed by Hu and Nuss in 1995 [20]. They used optically gated photoconductive antennas for the generation and detection of terahertz pulses. They replaced the slow scanning delay line used in THz-TDS systems with a rapid 20 Hz scanning delay line and used a digital signal processor instead of a lock-in amplifier (LIA) to acquire and digitise the signal. The sample was then scanned in x and y dimensions to build up an image. This system is shown in Fig. 1 and achieved an acquisition rate of 12 pixels/s with a signal-to-noise ratio greater than 100:1. This system was used to image leaves, bacon and semi-conductor circuits [9].

Shortly afterwards a dramatic improvement in acquisition speed was made using two-dimensional electro-optic detection of the terahertz pulse [21]. In this technique, the terahertz pulse acts as a transient bias on a $\langle 110 \rangle$ oriented ZnTe crystal, inducing a polarisation in the crystal. A probe laser pulse with a larger diameter than the THz beam is then

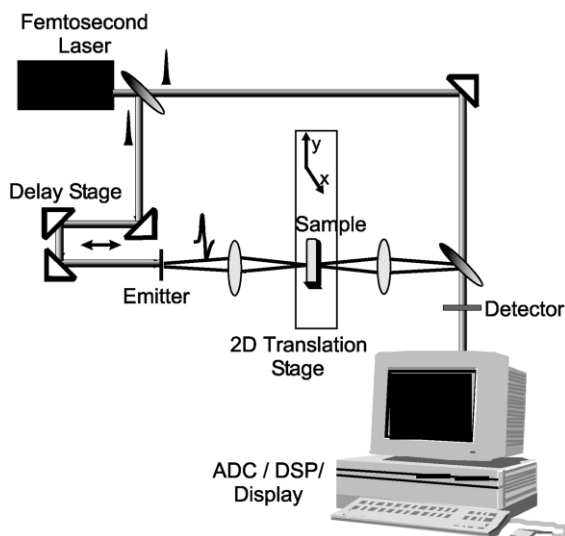


Fig. 1. Hardware schematic for scanned THz imaging [20]. The image is formed by scanning the mechanical motion stages in x , y and time dimensions.

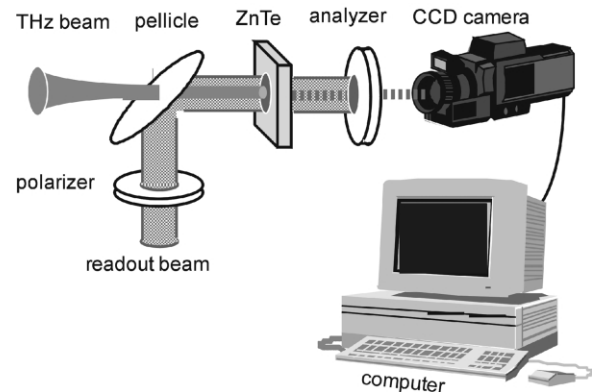


Fig. 2. Hardware schematic for all-optical 2D THz imaging [21]. The image is formed by expanding the THz and probe beams and using the Pockel's effect and crossed polarisers to convert the THz field to an intensity modulation which is measured using the CCD.

modulated by the polarisation-induced birefringence of the ZnTe crystal via the Pockel's effect. The two-dimensional THz field distribution is then converted to a 2D intensity modulation on the optical probe beam after it passes through a crossed polariser (analyser). A digital charge coupled device (CCD) camera is then used to record the optical image. This system is shown in Fig. 2.

2.1. THz imaging with a chirped probe pulse

Terahertz measurement using a chirped probe pulse is an innovative technique used to measure the full terahertz waveform simultaneously without the need for a scanning delay line. It is based on EO sampling [22], which is widely used for terahertz detection because of its wide bandwidth and sensitivity. In normal THz-TDS, the femtosecond laser pulse is used to probe the terahertz field at a certain time delay; the relative delay between the probe pulse and the terahertz pulse is then adjusted and the measurement repeated. In this way the full temporal profile of the terahertz pulse is measured as shown in Fig. 1. This process can be greatly accelerated by applying a linear chirp to the probe pulse. This is done using a diffraction grating. The different wavelength components of the incident pulse traverse different path lengths due to the variation in first order diffraction angle with wavelength, λ . The output from the grating is a pulse with an extended pulse duration and a wavelength that varies linearly with time.

In EO detection this chirped probe pulse is modulated by the THz pulse. In normal time scanning EO sampling a 100 fs optical pulse is modulated by a short temporal window of the THz pulse. The chirped probe pulse can be seen as a succession of short pulses each with a different wavelength. Each of these wavelength components encodes a different portion of the THz pulse simultaneously.

A spectrometer then spatially separates the different wavelength components and thus reveals the temporal THz pulse. The spatial signal output from the spectrometer is

then measured using a CCD. This technique derives from real time picosecond optical oscilloscopes [23,24].

2.2. Hardware setup

The hardware schematic for the chirped probe T-ray imaging system is shown in Fig. 3. A regeneratively amplified Ti:sapphire laser (Spectra Physics Hurricane) with an average output power of 700 mW, a pulse duration of 130 fs and a repetition rate of 1 kHz was used. The centre wavelength of the laser was 802 nm and the spectral bandwidth was 4 nm. The laser output was attenuated and split into pump and probe beams with powers of 30 mW and 20 μ W, respectively. The terahertz emitter was a GaAs photoconductive antenna. A bias of 1000 V was applied to the emitter electrodes which were spaced 16 mm apart. The average emitter current was 100 μ A. This system generated an average THz power of approximately 5 μ W (5 nJ per pulse). The THz beam was focused using parabolic mirrors to a spot size of 1 mm at the sample. The transmitted THz pulse was collected using parabolic mirrors and focused onto the 4 mm thick <110> ZnTe EO detector crystal.

The optical probe pulse was linearly chirped using the grating pair. The grating pair (grating constant 10 μ m) was setup to allow the grating separation to be varied which enabled us to investigate the effect of variable pulse width on the measurements. Nominally the grating separation was 4 mm and the angle of incidence was 51°, giving a chirped probe pulse width of 21 ps.

The chirped optical probe pulse and the terahertz pulse co-propagate in the ZnTe crystal as the group velocity of 800 nm light is approximately equal to the phase velocity of the THz field in ZnTe. During this time the polarisation of the wavelength components of the optical pulse are modulated differently, depending on the temporal profile of the THz pulse. Crossed polarisers are used to convert this polarization modulation to an amplitude modulation. The crossed polarisers ensure that the detected signal is approximately zero when no THz signal is present to prevent saturation of the CCD detector. Note that the background is not exactly zero due to laser scattering in

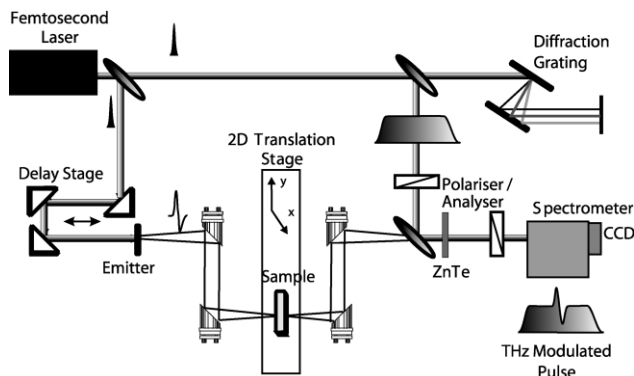


Fig. 3. Simplified hardware schematic used for terahertz imaging with a chirped probe pulse.

ZnTe, but this background is subtracted during processing (see Eq. (3)).

The temporal THz pulse is recovered by detecting the spectrum of the modulated pulse using a spectrometer grating (SPEX 500M) and a digital CCD camera (PI Pentamax) which has 384 \times 576 pixels and 12 bit encoder. The CCD was air cooled to -30 °C. Using a CCD exposure time of 100 ms the signal-to-noise ratio (SNR) for the system was approximately 180. The exposure time could be reduced down to 5 ms at the expense of SNR. The sample was mounted on a X–Y translation stage and raster scanned to acquire an image.

2.3. Mathematical model

Electro-optic detection with crossed polarisers imparts an amplitude modulation on the probe pulse. For relatively small modulation depths this modulation is linear and the modulated signal, $f_m(t)$, is given by

$$f_m(t) = f_c(t)[1 + kE(t - \tau)], \quad (1)$$

where $f_c(t)$ is the chirped probe pulse, k is the modulation constant, $E(t)$ is the terahertz electric field and τ is the relative time delay between the probe and THz pulse.

The spectrometer grating spatially disperses the different spectral components of the input signal. The signal detected at the CCD corresponding to a given frequency, $M(\omega_1)$, is given by the convolution of the spectral response function of the spectrometer grating, $g(\omega)$, with the square of the Fourier transform of the input signal, $f_m(t)$ [13]

$$M(\omega_1) \propto \int_{-\infty}^{\infty} g(\omega_1 - \omega) \left| \int_{-\infty}^{\infty} f_m(t) \exp(i\omega t) dt \right|^2 d\omega. \quad (2)$$

The normalised differential intensity is then defined as

$$N(\omega_1) = \frac{M(\omega_1)|_{\text{THz on}} - M(\omega_1)|_{\text{THz off}}}{M(\omega_1)|_{\text{THz off}}}. \quad (3)$$

Under certain assumptions $N(\omega_1)$ can be shown to be linearly proportional to the amplitude of the THz pulse, with the variable ω_1 proportional to the time, t . However, in most practical situations the THz signal is frequency band limited, which corresponds to a broadening of the temporal pulse.

Fig. 4 shows the THz signal measured using normal scanned electro-optic sampling and the chirped sampling method with a chirped pulse width of 21 ps. It is obvious that the THz pulse measured using the chirped probe pulse technique is significantly broadened. This broadening demonstrates the reduced temporal resolution and reduced frequency bandwidth of the chirped measurement technique compared with normal time scanned THz detection.

3. System identification

System identification refers to the problem of estimating a system that best describes the measured data. The measured

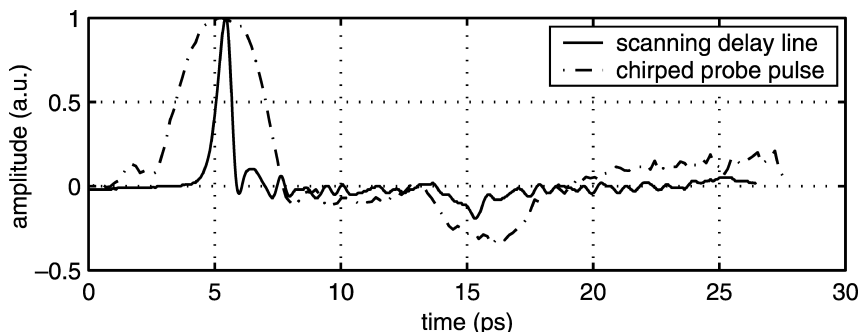


Fig. 4. Comparison of THz pulses measured with scanned EO sampling and EO sampling with a chirped probe pulse. The chirped pulse duration was 21 ps.

data is assumed to consist of two sets, $y(k)$ being the output of the unknown system when excited by the input signal $x(k)$. The signals considered here, $f(k)$, $k \in 0, \dots, N-1$, are real-valued, finite, discrete-time functions defined on the set of real numbers, \mathbb{R} . We consider the system S whose output depends on the input signal and on a noise signal $\nu(k)$

$$\mathbf{y} = S(\mathbf{x}, \nu). \quad (4)$$

The identification problem is to determine an estimator

$$\hat{\mathbf{y}} = \hat{S}(\mathbf{y}, \mathbf{x}), \quad (5)$$

which minimises some measure of the error signal

$$e(k) = y(k) - \hat{y}(k). \quad (6)$$

A common method of solving this problem is to assume that the predictor may be factored using a known transformation \hat{F} and a finite-dimensional parameter θ

$$\hat{S}(\mathbf{y}, \mathbf{x}) = \hat{S}(\mathbf{y}, \mathbf{x}, \theta), \quad (7)$$

which is then referred to as parametric system identification. Three common models used in this context are the finite impulse response (FIR) model

$$y(k) = - \sum_{i=0}^P c_i x(k-i) + \nu(k), \quad (8)$$

the autoregressive (AR) model

$$y(k) = - \sum_{j=0}^Q a_j y(k-j) + \nu(k), \quad (9)$$

and the ARX model which is a general class combining the two previous examples

$$y(k) = - \sum_{j=0}^Q a_j y(k-j) - \sum_{i=0}^P c_i x(k-i) + \nu(k), \quad (10)$$

where P and Q are the model orders. These models are easily understood as linear filters where the a_j and c_i represent the tap weights [25].

A large number of methods have been proposed to estimate the linear model coefficients [26]. In Section 4 we use an iterative least squares approach to identify appropriate model coefficients as a method of feature extraction in

order to classify the sample under test. For a given model, of order N , the model coefficients are used as the input to a simple classifier. We show that different tissue samples can be classified using this technique and evaluate the accuracy of the derived models. For this purpose, the THz pulse detected with no sample in place is considered to be the input, $x(k)$, and the THz pulse detected after transmission through the sample is taken as the system output, $y(k)$.

3.1. Classification

The ultimate goal in all terahertz systems is to extract information about the sample under test. This information may be the frequency dependent index of refraction for a semi-conductor wafer or the resonant absorption frequencies for gas sensing. For biological imaging applications we desire to detect and differentiate between different samples based on the terahertz response. We are interested in investigating our ability to perform such classification given an obtained image.

In this paper we use a simple classifier based on the Mahalanobis distance [27]. This is one of a class of minimum distance classifiers. It assumes that the data for each class are normally distributed, thus the samples drawn from each class will form a cluster in N dimensions, with a centre given by the mean vector, μ , and shape dependent on the covariance matrix, Σ . We form estimates of these parameters using the training vectors

$$\mu = E[\mathbf{x}], \quad (11)$$

$$\Sigma = E[(\mathbf{x} - \mu)(\mathbf{x} - \mu)^T]. \quad (12)$$

The Mahalanobis distance calculates the distance of a given point from the mean value for a given class normalised by the variance of the training vectors in that direction. For a class, k , the distance is defined as

$$d_k(\mathbf{x}) = (\mathbf{x} - \mu_k)^T \Sigma^{-1} (\mathbf{x} - \mu_k). \quad (13)$$

Classification is then performed by selecting the class for which the Mahalanobis distance is minimised. This classifier is optimal for normally distributed classes with equal covariance matrices and equal a priori probabilities. We are not claiming that the THz data conforms to these statistical assumptions, merely that this classifier represents

a useful starting point, as evidenced by the experimental results presented in Section 4.

This classification scheme was chosen because it is simple to implement and it provides reasonable results for a variety of statistical properties. More complicated classification algorithms abound and the appropriate choice for this application is an open research area. Simple neural network classifiers were also tested and found to yield similar results to those reported in Section 4.

There are several other promising classification techniques available. Supervised artificial neural networks (ANN) and support vector machines both have promise in the context of classifying THz wave data.

ANN are among the most popular classification architectures in use [28]. They derive their inspiration from the operation of human and animal brains which are based on a network of very simple building blocks called neurons. In a similar manner ANNs consist of a network of simple processing elements, which conventionally consist of a non-linear activation function applied to the sum of the weighted inputs. The weights of the neurons are adapted to the training data to train the neural network and then the classifier can be used to classify subsequent test vectors.

Support vector machines (SVMs) are a relatively recent approach to pattern recognition which have attracted a great deal of interest for a number of machine learning applications. SVM theory was first introduced by Vapnik [29] and is based on the principle of structural risk minimisation. Intuitively, given the set of samples belonging to two classes, SVMs learn the boundary between these two classes by mapping the input samples to a high dimensional space and then finding a hyperplane in this high dimensional space that separates the samples of the two classes. Computing the ideal hyperplane is posed as a constrained optimisation problem and solved using quadratic programming techniques.

4. Results

4.1. Imaging

A number of samples consisting of different biological tissues were imaged using the system described in Section 2.1. An emphasis was placed on biological tissue because biomedical imaging is an important potential application of this technology.

A dried butterfly was imaged to demonstrate the performance of the system. Fig. 5 shows an optical image of the sample. The sample was scanned using the chirped THz system with a scanning step size of 500 μm and a total range of 7 cm \times 7 cm. At each point the terahertz response was measured on the CCD using an exposure time of 100 ms. Thus the entire image was acquired in 32 min. To demonstrate the richness of the data obtained using this technique a number of images are shown in Fig. 6. In



Fig. 5. An optical image of the pressed butterfly sample used for chirped THz imaging.

Fig. 6(a) the peak amplitude of the THz pulse at each pixel was mapped to the grey scale intensity, for Fig. 6(b) each of the THz pulses were Fourier transformed to reveal the frequency domain information and the intensity of the spectra at a frequency of 0.2 THz was used as the grey scale intensity. Fig. 6(c) shows the phase information in the terahertz pulses by measuring the delay of the THz pulse at each pixel and then mapping this delay to the image intensity. Each of these three techniques yields different information about the sample under test and the optimal technique will depend on the desired application. These three images can be combined, for example, by mapping each to a different colour (red, green or blue) intensity to

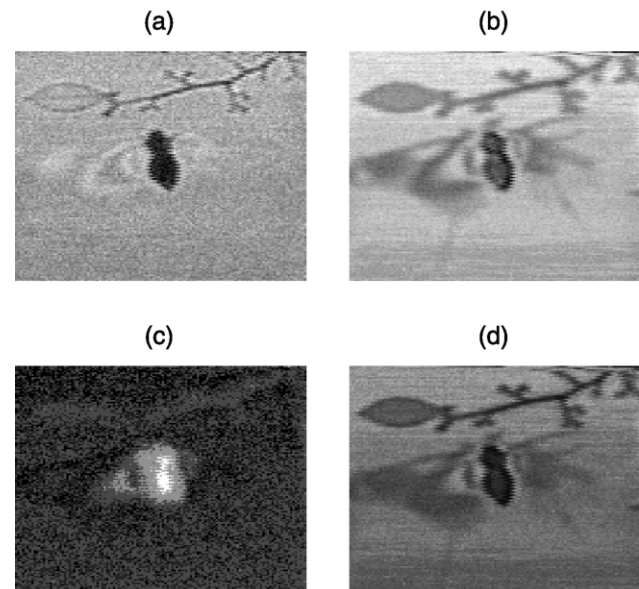


Fig. 6. Images of the pressed butterfly obtained using the chirped THz imaging technique. The data was obtained by scanning the sample in x (7 cm) and y (7 cm) dimensions with a resolution of 500 μm and measuring the THz response at each point. Image (a) was produced using the peak amplitude of the THz pulse at each pixel, image (b) was produced by taking the Fourier transform of the THz response and using the amplitude at 0.2 THz for each pixel, image (c) was produced by measuring the phase of the THz signal at each pixel and image (d) was produced by combining (a), (b) and (c).

produce a pseudo-colour image which may have biomedical diagnostic value, and an example is shown in Fig. 6(d).

A number of animal tissue samples were imaged. A beef sample was cut from a beef loin T-bone steak, parallel to the normal steak cut with a thickness of 1.5 mm. The sample was pressed and then dried in an oven for 12 h at 35 °C. For THz imaging the sample was held in a sample holder consisting of two 600 μm thick, high density polyethylene sheets. Polyethylene has negligible absorption in the THz band of interest and only marginal Fresnel loss due to its low refractive index. Samples of chicken tissue and chicken bone were obtained and imaged in a similar manner.

4.2. Linear modelling

Figs. 7 and 8 show the characteristic THz responses of the beef and chicken samples considered in both the time and frequency domain. The frequency limitation imposed by the chirped technique is evident. Using normal time scanned THz detection the THz bandwidth extends to 1.2 THz for the sample holder response.

Linear filter models of the sort discussed in Section 3 were employed for two reasons, firstly to attempt to infer information about the physical properties of the samples and secondly because the coefficients for an accurate model provide an efficient feature extraction method for the classification problem considered in Section 4.3.

An ensemble of 50 random responses for the chicken and beef samples were chosen. The model coefficients for various order AR and FIR models were then computed for each response. For each model the average coefficients were calculated and these used to calculate the percentage of the average actual response predicted by the model. These results are summarised in Table 1. Fig. 9 shows the second order FIR and AR filter model responses with the actual

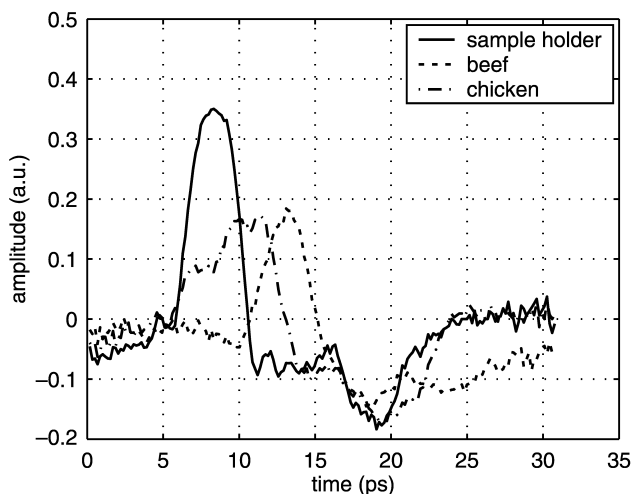


Fig. 7. The terahertz responses after transmission through the beef and chicken samples and the sample holder response. These responses were measured using the chirped measurement method with a CCD exposure of 100 ms.

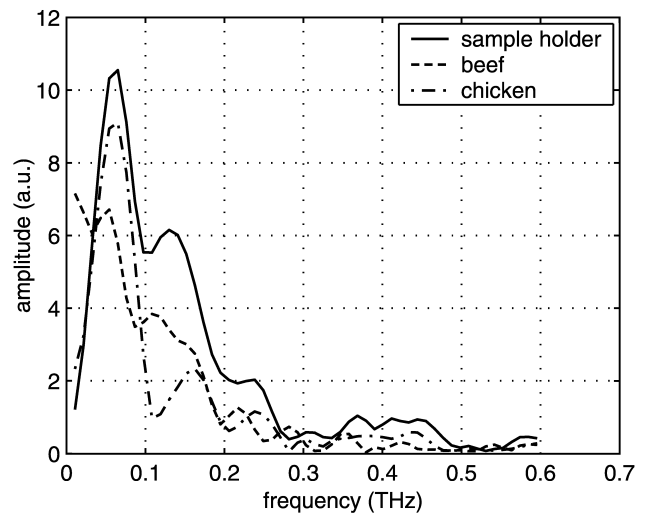


Fig. 8. The amplitude of the Fourier transform of the responses shown in Fig. 7. The frequency spectrum is limited to below 0.3 THz as discussed in Section 2.3.

chicken response. It can be seen that the model quite accurately represents the response of the sample.

4.3. Classification

The problem we considered was that of taking a random THz response and classifying it into one of three different classes: chicken, beef or empty sample holder. Training vectors were chosen at random from among the available responses. This example application is important for a number of reasons. Firstly the classification can be performed even if the samples are hidden in optically opaque containers, and secondly it demonstrates the potential of this technique for differentiating between more important materials such as normal and diseased tissue, or benign powders and bacterial spores.

Several different feature extraction methods were tested. It was found that the model coefficients for the FIR model proved to be very reliable features. The simple linear

Table 1
Prediction accuracy for different models

Model	Order	Prediction accuracy (%)
AR	2	30.0
AR	3	32.3
AR	4	35.5
AR	5	39.1
AR	6	42.9
FIR	2	43.4
FIR	3	51.0
FIR	4	53.1
FIR	5	56.5
FIR	6	59.4
ARX	2,2	44.8
ARX	3,3	59.8
ARX	4,4	64.6

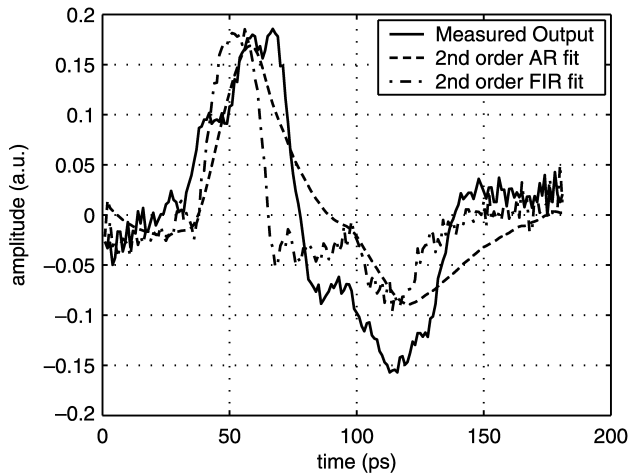


Fig. 9. Model output for second order FIR and AR filters and the actual response of the chicken sample. The models are quite accurate accounting for 43 and 32% of the actual response, respectively.

discriminant classifier described in Section 3.1 was trained using 50 pixel responses for each of the three classes. Three hundred random test responses were chosen and the classifier was used to assign them each to one of the classes. It was found that using the second order FIR coefficients as features resulted in successful classification of 297/300 while using the second order AR coefficients gave an accuracy of 289/300. An intuitively obvious feature extraction method involves simply using the amplitude of the THz pulse and the time at which the maximum amplitude occurred as features. These features give an indication of both the absorption and the phase-change induced by the sample under test. Using this feature extraction method only 283 of the 300 test vectors were accurately classified. The *confusion matrices* for these three classifiers are given in Eq. (14). The element, $[i,j]$, shows the relative proportion of samples belonging to class i that were recognised as class j :

$$\begin{aligned}
 \mathbf{X}_{\text{FIR}} &= \begin{bmatrix} 1 & 0 & 0 \\ 0 & 0.98 & 0.02 \\ 0 & 0.01 & 0.99 \end{bmatrix}, \\
 \mathbf{X}_{\text{AR}} &= \begin{bmatrix} 1 & 0 & 0 \\ 0 & 0.92 & 0.08 \\ 0 & 0.03 & 0.97 \end{bmatrix}, \\
 \mathbf{X}_{\text{amp}} &= \begin{bmatrix} 0.99 & 0.01 & 0 \\ 0 & 0.89 & 0.11 \\ 0 & 0.05 & 0.95 \end{bmatrix}.
 \end{aligned}
 \tag{14}$$

The classes were free air (1), beef (2) and chicken (3) pixels.

Figs. 10 and 11 demonstrate the benefits of the FIR model based approach by plotting the distribution of the

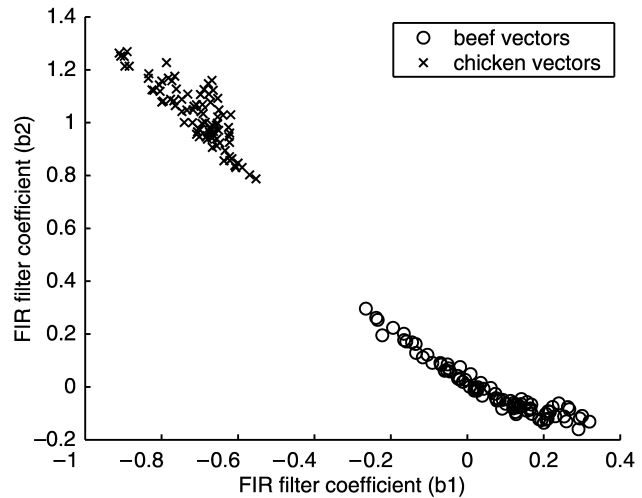


Fig. 10. Scatter plot showing the discriminating power of the second order FIR model coefficients. The optimal FIR model coefficients are found for 100 random samples and plotted. The two classes show a significant difference in their coefficients.

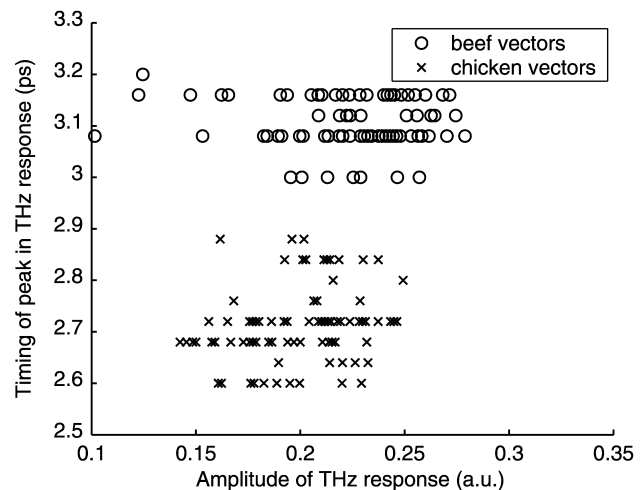


Fig. 11. Scatter plot showing the distribution of the peak amplitude and the timing of the peak of the THz pulses for beef and chicken samples. There is an obvious difference between the two tissue types but the separation of classes is not as strong as that shown in Fig. 10.

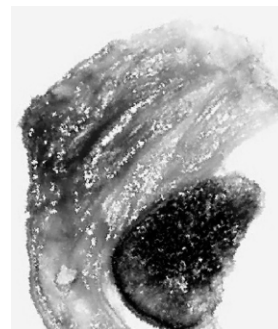


Fig. 12. A standard optical image of a sample of dried chicken tissue. The bone is clearly visible in the lower right of the image.

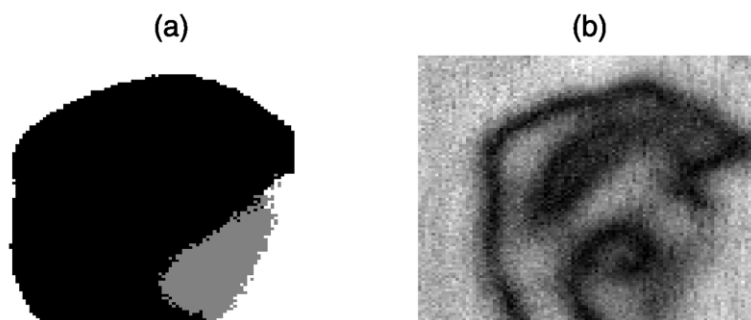


Fig. 13. Terahertz images of the chicken tissue shown in Fig. 12: (a) shows a pseudo-colour image generated by classifying each pixel of the image based on a number of training pixels which were chosen using knowledge of the original sample geometry; (b) shows a THz image generated by mapping the maximum amplitude of the THz pulse at each pixel to the grey scale intensity.

extracted features for a random set of beef and chicken pixels. The separation of the classes using the FIR model feature extraction method is visibly superior to the intuitive method described above.

The following example further illustrates the ability of the chirped probe pulse THz imaging technique to distinguish between biological tissues. It also highlights the ability of the algorithms described in this paper to assist in information extraction. A slice of chicken leg was cut so as to include a section of the bone. The sample was approximately 1.5 mm thick. The sample was then prepared and imaged as described in Section 4.1. An optical image of the sample is shown in Fig. 12. The terahertz data was analysed and it was found that the chicken and bone had a comparable absorption for THz signals and were not clearly distinguishable using standard intensity images. This is shown in Fig. 13(b) which shows the amplitude image of the chicken sample. To attempt to differentiate between the bone and tissue pixels in the image we used the simple Mahalanobis distance classifier and used fifth order FIR coefficients as input features. We trained the classifier based on 50 reference pixels for each class (bone, tissue and empty holder). The reference pixels were chosen based on the geometry of the sample. The classifier was then used to classify all 10,000 pixels of the image into one of the three classes. This classification was then used to colour code the image shown in Fig. 13(a). The bone area (grey) can be seen to accurately correspond to the bone in the optical image.

The computational complexity of the algorithms are a vital concern as systems head towards real-time data acquisition. The total time taken to classify the 10,000 responses in the image was less than 11 s on a Pentium IV PC with 256 MB of RAM. This is an order of magnitude less than the acquisition time for the same image and could be improved further by optimising the software implementation.

5. Conclusion

Terahertz imaging using a chirped probe pulse represents a recent addition to the available THz imaging techniques

and promises to allow terahertz imaging and spectroscopy to extend to new applications in the monitoring of ultrafast phenomena due to its capacity for single shot measurements.

We have presented the first ever images of biological tissue measured using this technique, and have demonstrated the richness of the information content of the obtained data. Simple feature extraction and classification algorithms were presented that allow for the automated analysis of these images and may one day facilitate computerised diagnosis of medical conditions based on the measured THz response. Beef and chicken samples were classified using a Mahalanobis distance classifier. The required computational complexity of the classifier was reduced using linear filter models to extract features from the measured responses. Different filter models were compared and very simple second order FIR filters were found to perform surprisingly well indicating that this model may be an accurate approximation of the underlying physical system. Further investigation of a physical model for the interaction of THz radiation with tissue is an important open question and it is likely to yield vastly improved feature extraction and classification algorithms.

The chirped imaging technique allows the full THz response of a single pixel to be measured simultaneously. This has advantages over all other THz imaging techniques in that if the sample moves during a scan the signature responses of the pixels are not corrupted, only the pixel to pixel intensity may change. Thus identification schemes such as those described in this paper will still succeed in classifying each pixel. However, the chirped imaging technique does suffer from a number of disadvantages. The measured response is not linearly dependent on the terahertz pulse as indicated in Section 2.3 and the signal-to-noise ratio is significantly higher than time-scanning techniques due to the absence of the lock-in amplifier. A number of solutions to the noise problem have been suggested including a lock-in CCD [30] and this remains an important focus of future research.

Acknowledgements

We appreciate communications with Dr Y. Chen (RPI) and Samuel Mickan (The University of Adelaide). This work was supported by the Australian Research Council, the US National Science Foundation and the US Army Research Office. Bradley Ferguson would like to thank the Australian–American Fulbright Commission.

References

- [1] D. Grischkowsky, S. Keiding, M. van Exter, C. Fattinger, Far-infrared time-domain spectroscopy with terahertz beams of dielectrics and semiconductors, *Journal of the Optical Society of America B: Optical Physics* 7 (10) (1990) 2006–2015.
- [2] R.H. Jacobsen, D.M. Mittleman, M.C. Nuss, Chemical recognition of gases and gas mixtures with terahertz waves, *Optics Letters* 21 (24) (1996) 2011–2013.
- [3] D. Arnone, C. Ciesla, M. Pepper, Terahertz imaging comes into view, *Physics World* (4) (2000) 35–40.
- [4] D.M. Mittleman, M. Gupta, R. Neelamani, R.G. Baraniuk, J.V. Rudd, M. Koch, Recent advances in terahertz imaging, *Applied Physics B: Lasers and Optics* 68 (6) (1999) 1085–1094.
- [5] S. Hadjiloucas, L.S. Haratzas, J.W. Bowen, Measurements of leaf water content using terahertz radiation, *IEEE Transactions on Microwave Theory and Techniques* 47 (2) (1999) 142–149.
- [6] M. Knott, See-through teeth, *New Scientist* 162 (2192) (1999) 22.
- [7] R.M. Woodward, B. Cole, V.P. Wallace, D.D. Arnone, R. Pye, E.H. Linfield, M. Pepper, A.G. Davies, Terahertz pulse imaging of in-vitro basal cell carcinoma samples, *Conference on Lasers and Electro-Optics 2001*, SPIE, 2001, p. 329–330.
- [8] C. Dahl, L. Genzel, P. Goy, G. Grüner, J.P. Kotthaus, G. Kozlov, M.C. Nuss, J. Orenstein, A. Volkov, Terahertz time-domain spectroscopy, in: G. Grüner (Ed.), *Millimeter and Submillimeter Wave Spectroscopy of Solids*, Springer, Berlin, 1998, pp. 7–50.
- [9] D.M. Mittleman, R.H. Jacobsen, M.C. Nuss, T-ray imaging, *IEEE Journal of Selected Topics in Quantum Electronics* 2(3) (1996) 679–692.
- [10] S. Mickan, D. Abbott, J. Munch, X.-C. Zhang, T. van Doorn, Analysis of system trade-offs for terahertz imaging, *Microelectronics Journal* 31 (7) (2000) 503–514.
- [11] Z. Jiang, X.-C. Zhang, Electro-optic measurement of THz field pulses with a chirped optical beam, *Applied Physics Letters* 72 (16) (1998) 1945–1947.
- [12] Z. Jiang, X.-C. Zhang, Single-shot spatiotemporal terahertz field imaging, *Optics Letters* 23 (14) (1998) 1114–1116.
- [13] F.G. Sun, Z. Jiang, X.-C. Zhang, Analysis of terahertz pulse measurement with a chirped probe beam, *Applied Physics Letters* 73 (16) (1998) 2233–2235.
- [14] J.A. Riordan, P.Y. Han, Z. Jiang, P. Campbell, Z.G. Lu, X.-C. Zhang, in: D.S. Citrin (Ed.), *THz beam sensors, OSA TOPS Radiative Processes and Dephasing in Semiconductors*, Washington, D.C., vol. 18, 1998, pp. 108–116.
- [15] B. Ferguson, D. Abbott, De-noising techniques for terahertz responses of biological samples, *Microelectronics Journal* 32 (12) (2001) 943–953.
- [16] B. Ferguson, D. Abbott, Wavelet de-noising of optical terahertz pulse imaging data, *Journal of Fluctuation and Noise Letters* 1 (2) (2001) L65–L69.
- [17] L. DuVillaret, F. Garet, J.-L. Coutaz, Highly precise determination of optical constants and sample thickness in terahertz time-domain spectroscopy, *Applied Optics* 38 (2) (1999) 409–415.
- [18] T.D. Dorney, R.G. Baraniuk, D.M. Mittleman, Material parameter estimation with terahertz time-domain spectroscopy, *Journal of the Optical Society of America A: Optics and Vision* 18 (7) (2001) 1562–1571.
- [19] D.M. Mittleman, R.H. Jacobsen, R. Neelamani, R.G. Baraniuk, M.C. Nuss, Gas sensing using terahertz time-domain spectroscopy, *Applied Physics B: Lasers and Optics* 67 (3) (1998) 379–390.
- [20] B.B. Hu, M.C. Nuss, Imaging with terahertz waves, *Optics Letters* 20 (16) (1995) 1716–1718.
- [21] Q. Wu, T.D. Hewitt, X.-C. Zhang, Two-dimensional electro-optic imaging of terahertz beams, *Applied Physics Letters* 69 (8) (1996) 1026–1028.
- [22] Q. Wu, X.-C. Zhang, Free-space electro-optic sampling of terahertz beams, *Applied Physics Letters* 67 (24) (1995) 3523–3525.
- [23] A. Galvanauskas, J.A. Tellefsen, A. Krotkus, M. Öberg, B. Broberg, Real-time picosecond electro-optic oscilloscope technique using a tunable semiconductor laser, *Applied Physics Letters* 60 (2) (1992) 145–147.
- [24] Z. Jiang, X.-C. Zhang, THz pulse measurement with a chirped optical beam, *Nonlinear Optics'98: Materials, Fundamentals and Applications Topical Meeting*, IEEE, Princeville, HI, USA, 1998, pp. 297–299.
- [25] S. Haykin, *Adaptive Filter Theory*, second ed., Prentice-Hall, Englewood Cliffs, NJ, 1991.
- [26] N. Kalouptsidis, S. Theodoridis (Eds.), *Adaptive system Identification and Signal Processing Algorithms*, Prentice-Hall, Hertfordshire, 1993.
- [27] J. Schürmann, *Pattern Classification—A Unified View of Statistical and Neural Approaches*, Wiley, New York, 1996.
- [28] S. Haykin, *Neural Networks—A Comprehensive Foundation*, Macmillan College Publishing, Englewood Cliffs, NJ, 1994.
- [29] V. Vapnik, *The Nature of Statistical Learning Theory*, Springer, New York, 1995.
- [30] Z. Jiang, X.-C. Zhang, Terahertz imaging via electrooptic effect, *IEEE Transactions on Microwave Theory and Techniques* 47 (12) (1999) 2644–2650.